EARTHQUAKE ENGINEERING AND STRUCTURAL DYNAMICS, VOL. 25, 1247–1257 (1996)

PROPERTY MATRICES IDENTIFICATION OF UNBOUNDED MEDIUM FROM UNIT-IMPULSE RESPONSE FUNCTIONS USING LEGENDRE POLYNOMIALS: IMPLEMENTATION AND EXAMPLES

ANTONIO PARONESSO AND JOHN P. WOLF

Department of Civil Engineering, Institute of Hydraulics and Energy, Swiss Federal Institute of Technology Lausanne, CH-1015 Lausanne, Switzerland

SUMMARY

The input and other implementation issues for the system identification procedure addressing the unit-impulse response matrix based on Legendre polynomials in the time domain to calculate the static—stiffness, damping and mass matrices of an unbounded medium are discussed. Clear guidelines are provided. High accuracy can be achieved even when the time range of the calculated unit-impulse response matrix is small (which may be necessary for computational efficiency) if the static—stiffness matrix is enforced.

KEY WORDS: Legendre polynomials; property matrices identification; rational approximation; soil–structure interaction; unbounded medium–structure interaction; unit-impulse response

1. INTRODUCTION

In an accompanying paper[1] starting from the *unit-impulse response matrix* corresponding to the degrees of freedom on the structure–medium interface of an unbounded medium the static-stiffness, damping and mass matrices are constructed, introducing a few internal variables. Thus, the unbounded medium is modelled in the same way as the structure is, enabling the same computer programme to be applied in a dynamic unbounded medium-structure-interaction analysis. Concepts of system identification are applied. The input and the output are expanded in a series of Legendre polynomials in the time domain which permits a rational approximation in the frequency domain of the dynamic-stiffness matrix to be determined. Only a system of linear equations is solved.

Various possibilities to choose the input are examined in the present paper as well as other implementation issues. Examples are also included to demonstrate the versatility of the method.

In Section 2 the influence of various parameters defining the input is systematically investigated. As the unit-impulse response matrix of the unbounded medium is only available up to a maximum time t_{max}, the output can also only be determined up to t_{max}. The effect of varying t_{max} is addressed. Various modifications to determine the rational approximation are examined such as enforcing the static-stiffness matrix, the initial value of the unit-impulse response matrix or predistorting the unit-impulse response matrix.

In Section 3 the out-of-plane (anti-plane) motion of a semi-infinite layer fixed at its base is examined. The high accuracy of this dispersive dynamic system with a cutoff frequency is demonstrated. The in-plane motion is also addressed.

In Section 4 conclusions including the optimum implementation of the procedure are stated.

Familiarity with the accompanying paper[1] is assumed. An equation in this article is referenced by the letter R (e.g. equation R(7)).

CCC 0098–8847/96/111247–11

Received 15 February 1996
Revised 25 May 1996

2. OPTIMUM IMPLEMENTATION

2.1. *Benchmark problem*

For the discussion addressing the optimum implementation, a simple one-dimensional case with an analytical solution is examined. The semi-infinite rod with area A, modulus of elasticity E, mass density ρ resting on an elastic foundation with the spring stiffness per unit length k_g is analysed (Figure 1). It presents a stringent test as this system is dispersive and exhibits a cutoff frequency. This one-dimensional system thus contains most properties present in a two- and three-dimensional system, where dispersion and cutoff frequencies often occur. Actually, the rod on elastic foundation models the dynamic behaviour of each mode of much more general cases. Waves propagating at an angle in a general system yield non-constant propagation velocities in the perpendicular direction which is also represented in the one-dimensional system by the non-constant phase velocity.

In this scalar case no diagonalization (Section 2 of Reference 1) needs to be performed. The superscript m is thus omitted.

The interaction force–displacement relationship at the beginning of the rod is formulated in the frequency domain as

$$R(\omega) = S(\omega)u(\omega) = \mathrm{i}\omega C_\infty + R_\mathrm{r}(\omega) \tag{1}$$

with the amplitudes of the displacement $u(\omega)$ and of the interaction force $R(\omega)$. The dynamic-stiffness coefficient is specified as

$$S(\omega) = K\sqrt{1 - \omega^2 \frac{A\rho}{k_g}} \tag{2}$$

with the static-stiffness coefficient $K = \sqrt{EAk_g}$ (Reference 2, p. 95). The dashpot coefficient describing the singular part equals $C_\infty = \rho c_l A$ ($c_l = \sqrt{E/\rho}$) and $R_\mathrm{r}(\omega)$ is the regular part. Specifying the dimensionless frequency $a_0 = \omega r_0/c_l = \omega\sqrt{A\rho/k_g}$ ($r_0 = \sqrt{EA/k_g}$) the dimensionless dynamic-stiffness coefficient is formulated as

$$\frac{S(a_0)}{K} = \sqrt{1 - a_0^2} \tag{3}$$

At the cutoff frequency $a_0 = 1$, $\mathrm{d}S(a_0)/\mathrm{d}a_0 = \infty$ holds. The regular part of the dynamic-stiffness coefficient equals

$$\frac{S_\mathrm{r}(a_0)}{K} = \sqrt{1 - a_0^2} - \mathrm{i}a_0 \tag{4}$$

It is customary to decompose the dynamic-stiffness coefficient into the dimensionless spring coefficient $k(a_0)$ and damping coefficient $c(a_0)$:

$$\frac{S(a_0)}{K} = k(a_0) + \mathrm{i}a_0 c(a_0) \tag{5}$$

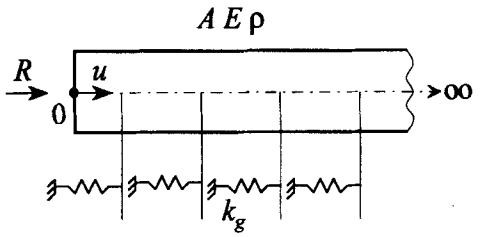

Figure 1. Semi-infinite rod on elastic foundation

In the time domain

$$R(t) = C_\infty \dot{u}(t) + R_r(t) \tag{6}$$

applies with the dashpot coefficient C_∞ describing the singular part, and the regular part of the interaction force is specified as

$$R_r(t) = \int_0^t S_r(t-\tau)u(\tau)\,d\tau \tag{7}$$

with the unit-impulse response coefficient

$$S_r(t) = K\frac{1}{t}J_1\left(\sqrt{\frac{k_g}{A\rho}}\,t\right) \tag{8}$$

(Bessel function of first order and first kind J_1). Specifying the dimensionless time $\bar{t} = tc_l/r_0 = t\sqrt{k_g/(A\rho)}$ the dimensionless unit-impulse response coefficient is written as

$$S_r(\bar{t})\frac{1}{K}\sqrt{\frac{A\rho}{k_g}} = \frac{1}{\bar{t}}J_1(\bar{t}) \tag{9}$$

(Reference 2, p. 344).

2.2. Selected input

The selection of the input $u^m(t)$, which is equal (after performing the diagonalization) to the transformed displacement, is discussed. It is desirable to achieve a uniform approximation of the regular part of the transformed dynamic-stiffness coefficient $S_r^m(\omega)$ for all ω. As is apparent from equation R(20), $u^m(\omega)$ acts as a weighting function on $S_r^m(\omega)$ when the output $R_r^m(\omega)$, which is equal to the regular part of the transformed force, is calculated. The system's frequency response is contained in $R_r^m(\omega)$. To reach a uniform contribution to $R_r^m(\omega)$ for all ω, the weighting function should be $u^m(\omega) = 1$ which corresponds to a Dirac delta function $\delta(t)$. When $u^m(\omega)$ favours a certain frequency band, the approximation will also be more accurate for these frequencies.

The selected input is formulated as

$$u^m(t) = a\frac{\alpha}{t_{max}}\,e^{(-\alpha/t_{max})t}H(t) \tag{10}$$

with the Heaviside step function $H(t)$; α is dimensionless. The constant a, with the dimension length times time, represents the integral $\int_0^\infty u^m(t)\,dt$ which is selected as one and is thus independent of α. For the limit $\alpha \to \infty$, $u^m(t)$ tends to the Dirac delta function $\delta(t)$. The more α diminishes, the more emphasis is placed on $u^m(\omega)$ at small ω at the cost of that at large ω.

The case where the time t_{max} up to which the unit-impulse response is available is sufficiently large is examined. From a practical point of view, $u^m(t)$ will be negligible for $t > t_1$. It is assumed that $S_r^m(t)$ can be set equal to zero for $t > t_2$ which corresponds to complete data. It follows that $R_r^m(t)$ will also be zero for $t > t_1 + t_2$. t_{max} is selected as larger than $t_1 + t_2$ for the discussion.

The rod on elastic foundation is used to illustrate the effect of α for a fixed $\bar{t}_{max} = t_{max}c_l/r_0 = 30$. The degree of the polynomial in the denominator of the rational approximation $S_r(i\omega)$ (equation R(34)) is chosen as $M = 4$. The number of terms used in the Legendre expansion of the input and the output (equations R(37) and R(38)) is selected as $l = 30$. The input parameters $\alpha = 400$, $= 100$, and $= 10$ are processed.

For $\alpha = 100$ the input $u(\bar{t})$ is compared to its Legendre polynomials expansion in Figure 2(a) and the output $R_r(\bar{t})$ in Figure 2(c). The error of the input (after normalization with the maximum value of $u(\bar{t})$) denoted as $e_u(\bar{t})$ is shown in Figure 2(b) and the error of the output in Figure 2(d). For the selected number of terms in the Legendre polynomials expansion $l = 30$, the accuracy is excellent.

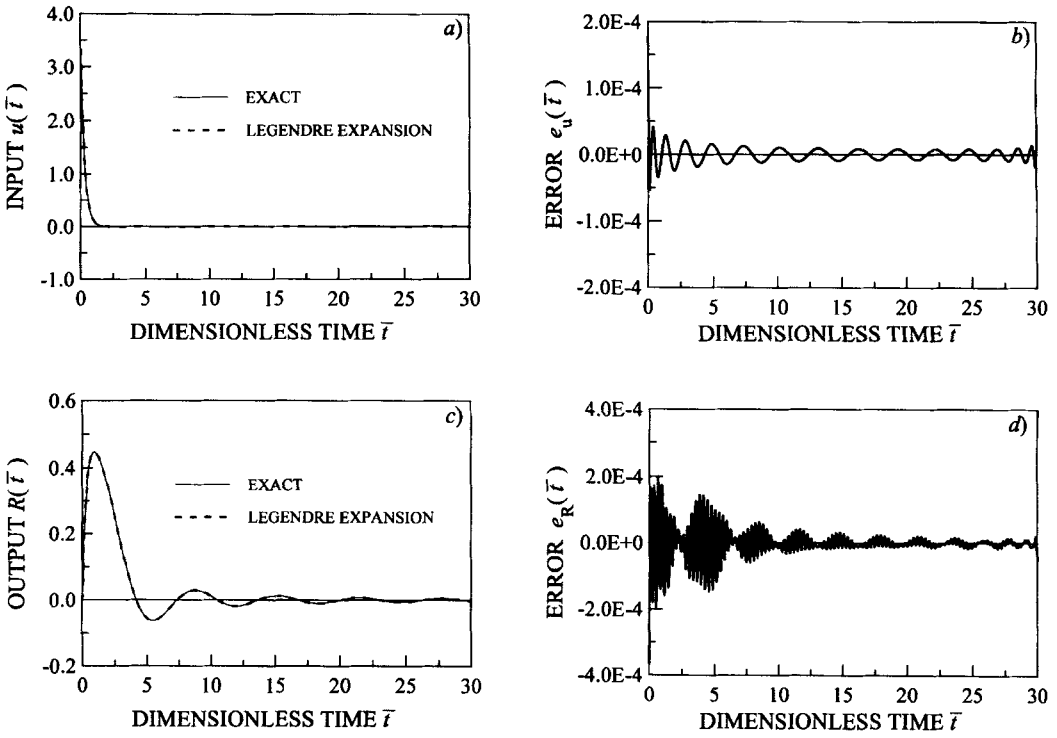

Figure 2. Accuracy of Legendre polynomials expansion: (a) input; (b) error of input; (c) output; (d) error of output

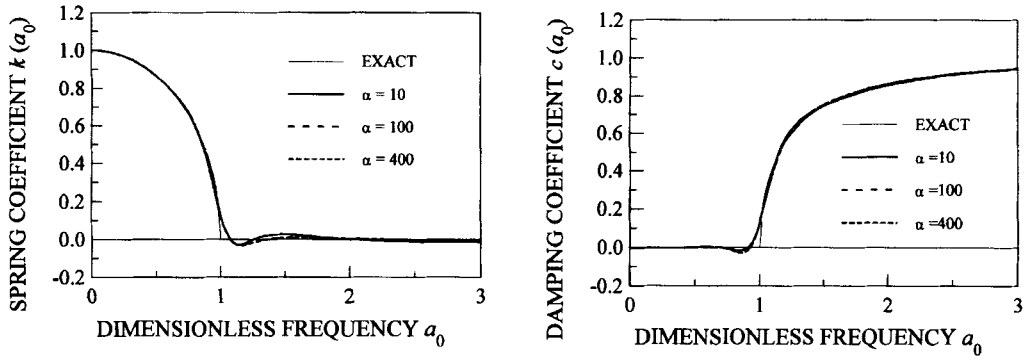

Figure 3. Influence of selected input parameter α on dynamic-stiffness coefficient for $\bar{t}_{max} = 30$

A comparison of the dynamic-stiffness coefficient $S(a_0)$ decomposed as in equation (5) with the exact solution of equation (3) is shown in Figure 3. The magnitude of the error $\varepsilon(a_0)$ defined as the difference of the approximated and exact regular parts of the dynamic-stiffness coefficient is plotted in Figure 4 together with the magnitude of the Fourier transform $u(a_0)$ of $u(\bar{t})$ in equation (10).

As expected, the approximation deviates most at $a_0 = 1$, the cutoff frequency. As already mentioned the limit for $a_0 \to \infty$ is exact. For $\alpha = 100$ where the weighting function $u(a_0)$ is more uniform in magnitude than that for $\alpha = 10$ the error in the intermediate-frequency range is smaller but larger in the low-frequency range. The corresponding comparison of the regular parts of the unit-impulse response coefficients $S_r(\bar{t})$ normalized as in equation (9) is shown for early times in Figure 5. For $\alpha = 100$ (which leads to more accurate results in

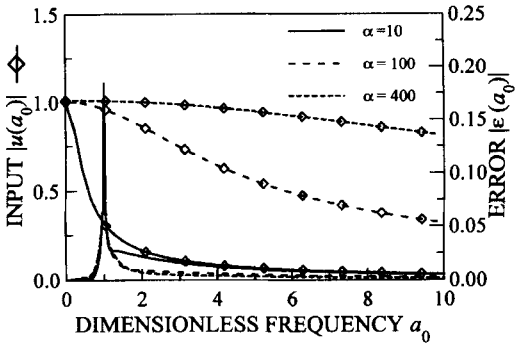

Figure 4. Influence of selected input parameter α on error of dynamic-stiffness coefficient: ($\diamond$) magnitude of amplitude $u(a_0)$; (——) magnitude of error amplitude $\varepsilon(a_0)$

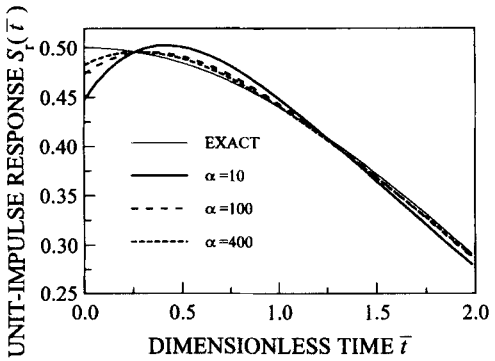

Figure 5. Influence of selected input parameter α on regular part of unit-impulse response coefficient shown for $\bar{t} \leqslant 2$ for $\bar{t}_{max} = 30$

the intermediate-frequency range) the agreement is better in the early-time range than for $\alpha = 10$. For late times the differences are minor (not shown).

The weighting effect is, however, not pronounced. As expected, the parameters of the system are hardly affected by the choice of the input.

The use of the input defined in equation (10) permits by reducing α to achieve a somewhat better approximation in the low-frequency range. This can be desirable for certain seismic excitations. When a good approximation is also necessary in the intermediate-frequency range, an input defined as a Dirac delta function $\delta(t)$ (corresponding to $\alpha = \infty$) could be selected. This case is discussed.

For a Legendre polynomials expansion of $\delta(t)$ the coefficients equal (equation R(39)

$$c_{ui} = \frac{2i+1}{t_{max}} \varphi_i(0), \quad i = 0, \ldots, l-1 \tag{11}$$

with the Legendre polynomials at $t = 0$

$$\varphi_i(0) = (-1)^i \tag{12}$$

The convolution integral to determine the output (equation R(19)) is avoided, as

$$R_r^m(t) = S_r^m(t) \tag{13}$$

applies, i.e. a Legendre polynomials expansion is calculated directly for $S_r^m(t)$.

It follows from equations (11) and (12) that the c_{ui} increase in absolute value for increasing i (for a finite α using equation (10) the c_{ui} tend to zero for a sufficiently large i). Numerical experience indicates that to counteract this effect the ith row of the overdetermined system of equation R(44) must be multiplied by $1/|c_{ui}| = t_{max}/(2i + 1)$. Thus, a weighted least-squares approximation is performed with a diagonal weighting matrix.

For illustration, the semi-infinite rod on an elastic foundation with $M = 4$, $l = 30$ and $\bar{t}_{max} = 30$ is addressed again. Both the dynamic-stiffness coefficient $S(a_0)$ (Figure 3) and the regular part of the unit-impulse response coefficient $S_r(\bar{t})$ (Figure 5) using $\delta(t)$ as input coincide from a practical point of view with the case $\alpha = 400$.

2.3. *Varying time range of unit-impulse response coefficient*

For a $\delta(t)$ as input, t_1 defined in the paragraph following equation (10) will vanish. The maximum time t_{max} up to which the unit-impulse response matrix is calculated must be limited for computational efficiency. Thus, $S_r^m(t)$ is not available up to t_2. In this case of an approximation with partial data, t_{max} will be significantly smaller than t_2. As a consequence, the approximation using the expansion in Legendre polynomials is accurate for $t \leqslant t_{max}$. For $t > t_{max}$ no control exists which can yield an inaccurate approximation. It follows that the approximate $S_r^m(ia_0)$ is accurate for the intermediate frequencies (and the high-frequency range) and potentially inaccurate for low frequencies.

For demonstration, the semi-infinite rod on an elastic foundation with $M = 4$, $l = 30$ and $\bar{t}_{max} = 5$ using the Dirac delta function $\delta(t)$ as input is examined. For this very stringent test large deviations exist in $S_r(\bar{t})$ for $\bar{t}_{max} > 5$ (Figure 7) which results in an inaccurate $S_r(ia_0)$ for $a_0 < 1$ in Figure 6. To improve the approximation for low frequencies, the following measures can be taken: the static-stiffness coefficient is enforced or a predistortion is introduced.

2.4. *Enforcing static-stiffness coefficient*

The static-stiffness coefficient can be enforced as described in equation R(52). A drastic improvement (Figures 6 and 7) results using the same parameters.

2.5. *Predistortion of the unit-impulse response coefficient*

The regular part of the unit-impulse response coefficient can be predistorted as discussed in connection with equations R(55) and R(56). For $\beta = 160$ the behaviours at low frequencies (Figure 6) and at intermediate times (Figure 7) improve.

2.6. *Enforcing initial value of regular part of unit-impulse response coefficient*

For a large $\bar{t}_{max}$, enforcing the initial value of the regular part of the unit-impulse response coefficient improves the accuracy for early times (not shown).

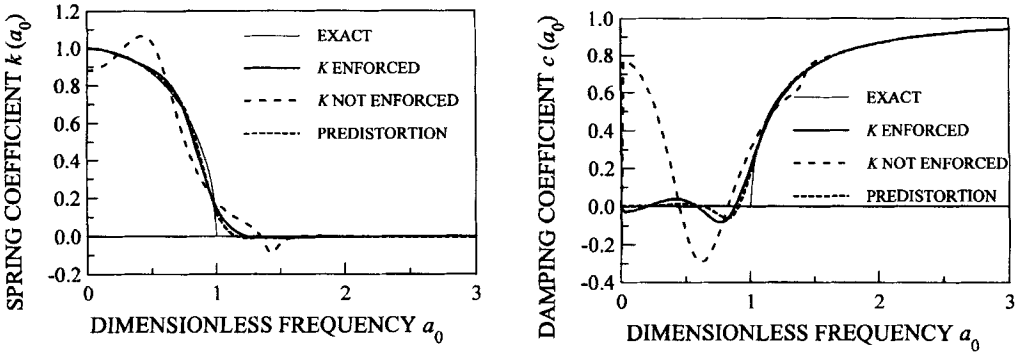

Figure 6. Influence of enforcing static-stiffness coefficient and predistortion on dynamic-stiffness coefficient for $\bar{t}_{max} = 5$

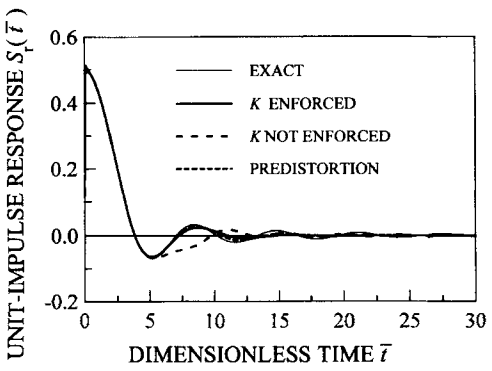

Figure 7. Influence of enforcing static-stiffness coefficient and predistortion on regular part of unit-impulse response coefficient for $\bar{t}_{max}=5$

3. SEMI-INFINITE LAYER FIXED AT ITS BASE

As an example of practical importance the out-of-plane (anti-plane) motion of a semi-infinite layer with a free and a fixed boundary extending to infinity of constant depth d, shear modulus G and mass density ρ is examined (Figure 8). The structure–medium interface is perpendicular to the boundaries extending to infinity.

Based on the method of separation of variables an analytical solution for the dynamic-stiffness matrix $[S(a_0)]$ and the unit-impulse response matrix $[S(\bar{t})]$ can be derived where $\bar{t} = tc_s/d$ is the dimensionless time (shear-wave velocity $c_s=\sqrt{G/\rho}$) and $a_0 = \omega d/c_s$ the dimensionless frequency.

This dynamic system is dispersive with a cutoff frequency of $a_0 = \pi/2$. To ease comparison, 5 line elements of equal length $d/5$ with piecewise linear displacements are introduced. The numbers of the nodes are shown in Figure 8.

As input the exponential function (equation (10)) with $\alpha=10$ is selected. The number of terms in the Legendre polynomials expansion is fixed at $l=30$. The degree of the polynomial in the denominator of the rational approximation (equation R(34)) is first chosen as $M=12$. If an unstable system with a positive real part of a pole occurs (as explained in connection with equation R(57)), M is reduced by 1 and the overdetermined system (equation R(44)) is reformulated and solved again. This procedure is repeated until a stable system occurs. The maximum time $\bar{t}_{max}$ is varied ($=10$ and 2). The static-stiffness coefficient K^m is also enforced sometimes. The coefficients (1, 1) and (1, 5) are compared, i.e. $S_{11}(a_0)$, $S_{r11}(\bar{t})$ and $S_{15}(a_0)$, $S_{r15}(\bar{t})$. Both total dynamic-stiffness coefficients of the original matrix are non-dimensionalized by the static-stiffness coefficient K_{11} and then decomposed into dimensionless spring coefficients $k(a_0)$ and damping coefficients $c(a_0)$. Both regular parts of the unit-impulse response coefficients of the original matrix are non-dimensionalized by $K_{11}c_s/d$.

First, $\bar{t}_{max}=10$ is selected without enforcing the static-stiffness coefficient K^m (Figures 9 and 10); high accuracy results. In particular, the low-frequency range is better represented than the intermediate range. As the deviation of the static-stiffness coefficient is small, enforcing K^m hardly affects the results (not shown). Note that the effect of the retarded time in $S_{r15}(\bar{t})$ (Figure 10(b)) is modelled in the average only.

Second, $\bar{t}_{max}$ is reduced to $=2$ without enforcing the static-stiffness coefficient K^m (Figures 9 and 10). The accuracy in the low-frequency range is reduced and in the intermediate frequency range increased. The static-stiffness coefficient is, in general, not well represented (Figure 9(a)). Substantial deviations for $\bar{t} > \bar{t}_{max}=2$ in $S_r(\bar{t})$ arise but the effect of the retarded time in $S_{r15}(\bar{t})$ is captured well (Figure 10(b)).

Third, $\bar{t}_{max}=2$ is kept but K^m is enforced (Figures 11 and 12). The accuracy is improved throughout the frequency range.

As an extension the in-plane motion of a semi-infinite layer with a free and a fixed boundary extending to infinity of constant depth d, shear modulus G, Poisson's ratio $=\frac{1}{3}$ and mass density ρ is addressed (Figure 13).

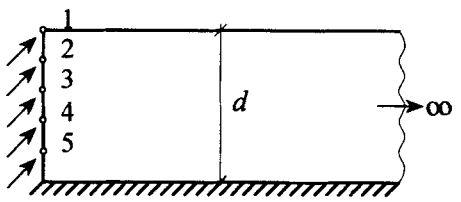

Figure 8. Out-of-plane motion of semi-infinite layer fixed at its base with discretization on structure–medium interface

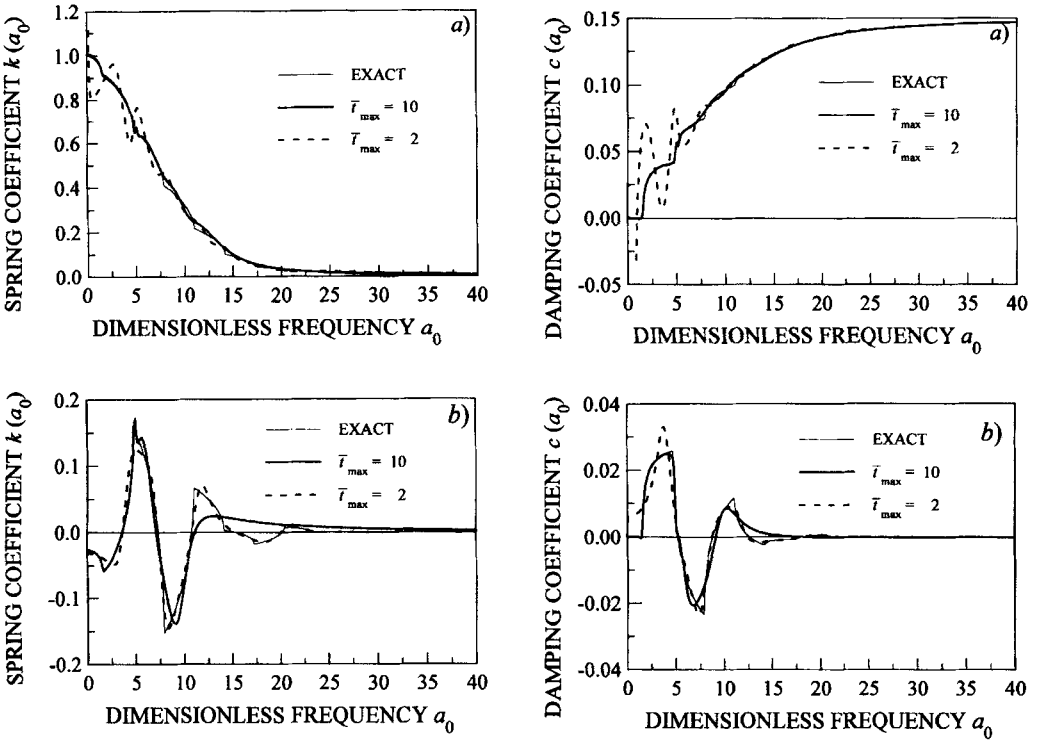

Figure 9. Dynamic-stiffness coefficient of out-of-plane motion with K^m not enforced: (a) element $S_{11}(a_0)$; (b) element $S_{15}(a_0)$

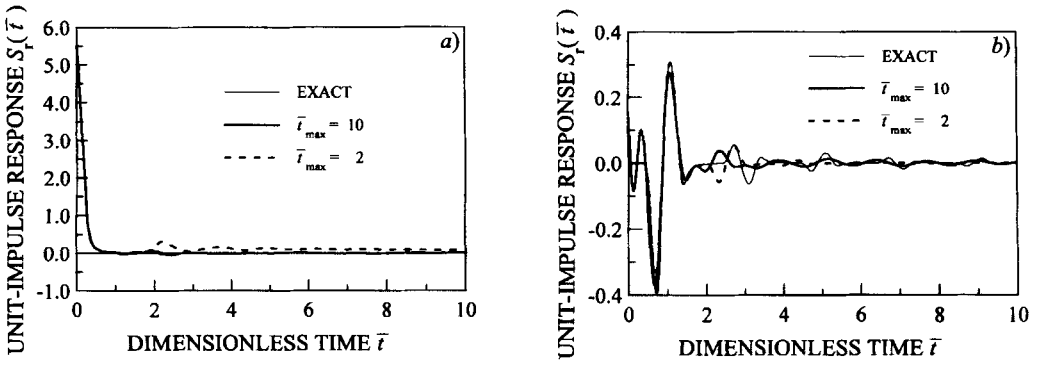

Figure 10. Regular part of unit-impulse response coefficient of out-of-plane motion with K^m not enforced: (a) element $S_{r11}(\bar{t})$; (b) element $S_{r15}(\bar{t})$

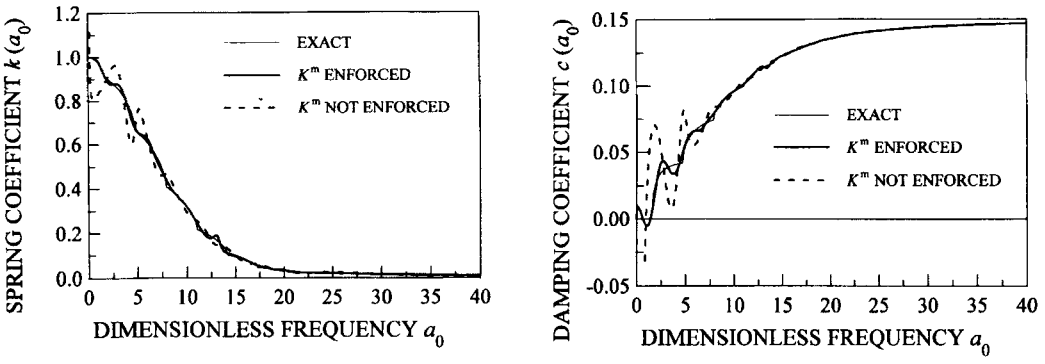

Figure 11. Dynamic-stiffness coefficient $S_{11}(a_0)$ of out-of-plane motion with $\bar{t}_{max}=2$

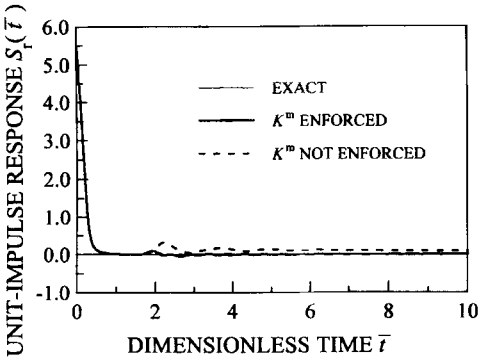

Figure 12. Regular part of unit-impulse response coefficient $S_{r11}(\bar{t})$ of out-of-plane motion with $\bar{t}_{max}=2$

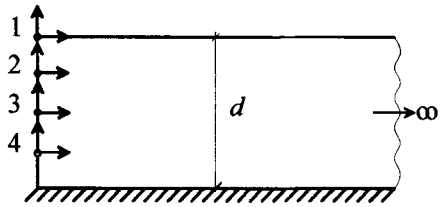

Figure 13. In-plane motion of semi-infinite layer fixed at its base with discretization on structure–medium interface

On the vertical structure–medium interface 8 line finite elements, each with 3 nodes, are introduced (not shown) in the consistent infinitesimal finite-element cell method.[3] This discretization permits an adequate modelling up to the dimensionless frequency $a_0 = \omega d/c_s = 2{\cdot}5\pi$ ($c_s = \sqrt{G/\rho}$). To reduce the data for the examination, 4 nodes with the numbers shown in Figure 13 with piecewise linear displacements are introduced, and the corresponding reduction is performed based on virtual-work considerations. This leads to the corresponding matrices $[S_r(\bar{t})]$ and $[S(a_0)]$ of order 8×8 with the dimensionless time $\bar{t} = tc_s/d$. These results are denoted as rigorous. The cutoff frequency of the layer corresponds to $a_0 = \pi/2$. The analysis is performed for the degree of the rational approximation $M = 12$, and the number of terms in the Legendre expansion is selected as $l = 40$. The maximum dimensionless time is equal to $\bar{t}_{max} = 10$. As input, the exponential function specified in equation (10) with $\alpha = 10$ is chosen. The static-stiffness coefficient is not enforced.

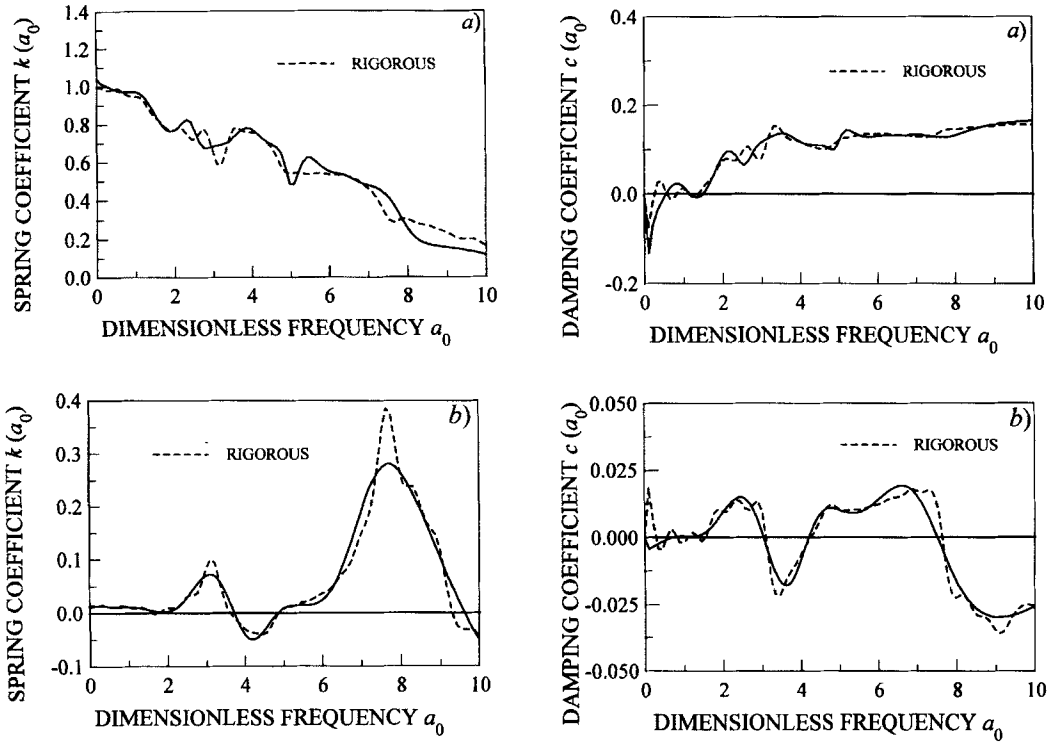

Figure 14. Dynamic-stiffness coefficient of in-plane motion: (a) element $S_{11}(a_0)$; (b) element $S_{18}(a_0)$

To check the accuracy in the frequency domain, the total dynamic-stiffness coefficient $S_{11}(a_0)$, relating the horizontal displacement in node 1 to the horizontal interaction force in the same node, and $S_{18}(a_0)$, relating the vertical displacement in node 4 to the horizontal interaction force in node 1, are examined. Both dynamic-stiffness coefficients are non-dimensionalized by the static-stiffness coefficient K_{11} and then again decomposed into a spring coefficient $k(a_0)$ and a damping coefficient $c(a_0)$. From the comparison shown in Figure 14, it follows that although the rigorous results vary significantly the rational approximation up to $a_0 = 10$ is good also for the in-plane motion.

4. CONCLUSIONS

1. The rational approximation and thus the static-stiffness, damping and mass matrices representing the unbounded medium are hardly affected by the choice of the input. Both exponential functions with varying decay factors and the Dirac delta function can be applied.
2. For a large time range of the unit-impulse response matrix (t_{max} large, complete data) excellent accuracy, in particular in the low-frequency range, is achieved. No need exists to enforce the static-stiffness matrix. In the time domain, discrepancies do occur; in particular, the retarded time effect is modelled only in the average. Enforcing the initial value of the regular part of the unit-impulse response matrix improves the approximation.
3. For a small time range of the unit-impulse response matrix (t_{max} small, partial data) the accuracy deteriorates, in particular in the low-frequency range. Enforcing the static-stiffness matrix improves the accuracy dramatically throughout the frequency range. In the time domain, excellent accuracy results up to t_{max}. No need exists to enforce the initial value of the regular part of the unit-impulse response matrix.

4. For a small computational effort the unit-impulse response matrix can be computed for a small time range only. The presented system identification method using Legendre polynomials in the time domain and enforcing the static-stiffness matrix results in a competitive procedure to calculate the static-stiffness, damping and mass matrices of the unbounded medium.

REFERENCES

1. A. Paronesso and J. P. Wolf, 'Property matrices identification of unbounded medium from unit-impulse response functions using Legendre polynomials: formulation', *Earthquake eng. struct. dyn.*, **25**, 1231–1245 (1996).
2. J. P. Wolf, *Soil–Structure-Interaction Analysis in Time Domain*, Prentice-Hall, Englewood Cliffs, NJ, 1988.
3. C. Song and J. P. Wolf, 'Consistent infinitesimal finite-element cell method: Three-dimensional vector wave equation', *Int. j. numer. methods eng.* **39**, 2189–2208 (1996).